nature climate change

SUPPLEMENTARY INFORMATION

DOI: 10.1038/NCLIMATE2873

Multi-scale predictions of massive conifer mortality due to chronic temperature rise

N.G. McDowell, A.P. Williams, C. Xu, W.T. Pockman, T. Dickman, S. Sevanto, R. Pangle, J. Limousin, J. Plaut, D. Scott Mackay, J. Ogee, J.C. Domec, C.D. Allen, R.A. Fisher, X. Jiang, J. Muss, D.D. Breshears, S. A. Rauscher, C. Koven

Author contributions

[1]Contributed to development of the project and critical important contribution to analysis

[2]Contributed to field work critical to the project

[3]Contributed to model simulations and data analysis critical to the project

[1,2]N.G. McDowell, [1,3]A.P. Williams, [1,3]C. Xu, [1]W.T. Pockman, [2]T. Dickman, [2]S. Sevanto, [2]R. Pangle, [2]J. Limousin, [2]J. Plaut, [1,3]D. Scott Mackay, [1,3]J. Ogee, [1,3]J.C. Domec, [1]C.D. Allen, [1,3]R.A. Fisher, [1,3]X. Jiang, [3]J. Muss, [1,2]D.D. Breshears, [1,3]S. Rauscher, [3]C. Koven

Material and methods. Material provided in the order of presentation in the main text.

SI 1: Figure 1a description

SI 2: Figure 1b description

SI 3: Equation (1) assumptions

SI 4: Influence of temperature and specific humidity on vapor pressure deficit

SI 5: Methods associated with Figure 2

SI Figure S1, and associated predictive equations for Ψ_{pd}

SI 6: Regressions for Figure 2.

SI 7: References regarding foliar starch

SI Figure S2

SI 8: Model-specific developments, application, and full descriptions (associated with Figure 3)

SI Figure S3

SI Figure S4

SI Figure S5

SI 9: Calculations of mortality probability (associated with Figure 3)

SI Figure S6

SI Figure S7

DOI: 10.1038/NCLIMATE2873

SI 10: Methods associated with Figure 4.

SI 1: Figure 1a shows the trend in mortality over time from five regions. These data were previously published in [2,7] and were graciously provided by the lead authors.

SI 2: Figure 1b shows predictions of stomatal conductance from equation (1) using a range of soil water potentials and an assumed vapor pressure deficit of 1 kPa, with anisohydric species water potential gradient declining with soil water potential at 50% the rate of the isohydric species. Anisohydric species are rare amongst NET species, with juniper being amongst the most widespread and drought tolerant. Pines, in contrast, are relatively isohydric (for example [20]).

SI 3: Equation (1) is a fundamental tenet of plant hydraulic theory and has been validated in numerous studies. Most importantly, it has been validated with high rigor and accuracy in field studies (the scale of interest to this study) by Whitehead et al 1984, Whitehead 1998, Oren et al. 1999, McDowell et al. 2006, 2008 and Phillips et al. 2002. Equation (1) assumes that vegetation tends toward space-filling relationships (West et al. 1999) that optimize carbon gain for water loss (Cowan and Givnish 1986). Papers in support of Darcy's law derived for trees (equation 1):

McDowell NG, White S, Pockman WT. Transpiration and stomatal conductance across a steep climate gradient in the southern Rocky Mountains. *Ecohydrology*, **1**:193-204. (2008)

McDowell NG, Adams HA, Bailey JD, Hess M, Kolb TE. Homeostatic maintenance of ponderosa pine gas exchange in response to stand density changes. Ecol Appl **16**(3):1164-1182 (2006)

Oren R, Sperry JS, Katul GG, Pataki DE, Ewers BE, Phillips N, Schäfer K VR. Survey and synthesis of intra- and interspecific variation in stomatal sensitivity to vapour pressure deficit. Plant Cell and Environ **22:** 1515-1526. (1999)

Phillips N, Bond BJ, McDowell NG, Ryan MG. Canopy and hydraulic conductance in young, mature and old Douglas-fir trees. Tree Physiol **22**:205-211 (2002)

Whitehead D, Edwards WRN, Jarvis PG. Conducting sapwood area, foliage area, and permeability in mature trees of *Picea sitchensis* and *Pinus contorta*. Can J For Res **14**:940-947. (1984)

Whitehead D. Regulation of stomatal conductance and transpiration in forest canopies. *Tree Physiol*. **18**:633-644. (1998)

Cowan I. R., Givnish T. J., Economics of carbon fixation in higher plants, in *On the economy of plant form and function* (Cambridge University Press, Cambridge, 1986), pp. 133-170.

West G.B., Brown J.H., Enquist B.J., A general model for the structure and allometry of plant vascular systems. *Nature* **400**, 664-667 (1999).

SI 4: Rising temperature causes a rise in vapor pressure deficit (Breshears et al. 2013; Trenberth et al. 2013; Williams et al. 2013) despite rising absolute humidity associated with increased global evaporation (Held and Sodden 2006). Example calculations are shown in both Breshears

et al. 2013 and McDowell and Allen 2015. This rise in vapor pressure deficit with rising temperature results from the larger rise in saturation vapor pressure than the projected rise in actual vapor pressure due to the non-linear Clausius-Clapeyron relationship between temperature and saturation vapor pressure. This effect is enhanced over land surfaces because of the increase in the ratio of sensible to latent heat fluxes caused by reduced evaporation over land during drought (Maness et al. 2013).

The example calculations from McDowell and Allen 2015 are shown here.

Vapor pressure deficit (D) is defined here as the difference in vapor pressure or mole fraction between sub-stomatal air (es(Ts)) and ambient air after correction for the shift in humidity (rh):

$$D = \mathrm{es}(Ts)(1 - rh).$$

From the Clausius-Clapeyron equation we can calculate *es(Ts)* as:

$$(ts) = a \exp(bt/t+c),$$

where a = 0.611kPa, b=17.502, and c=240.97°C. We assume for this calculation that the sub stomatal pore is saturated. If we assume a 4% increase in *rh* (Harris et al. 2014) with a shift in temperature from 30 to 35°C, then *D* will rise from 2.97 to 3.71 kPa, or a 20% rise in *D*.

D.D. Breshears, H.D. Adams, D. Eamus, N.G. McDowell, D.J. Law, R.E. Will, A.P. Williams, C.B. Zou. The critical amplifying role of increasing atmospheric moisture demand on tree mortality and associated regional die-off. *Frontiers in plant science* 4 (2013).

Harris, I., Jones, P.D., Osborn, T.J., and Lister, D.H. (2014), Updated high-resolution grids of monthly climatic observations - the CRU TS3.10 Dataset. Int. J. Climatol.,34: 623-642. Doi:10.1002/joc.3711

I.M. Held, B.J. Soden. Robust responses of the hydrological cycle to global warming. *Journal of Climate* 19, no. 21 5686-5699 (2006).

H. Maness, P.J. Kushner, I. Fung. Summertime climate response to mountain pine beetle disturbance in British Columbia. *Nature Geoscience* 6, no. 1, 65-70 (2013).

N.G. McDowell, C.D. Allen. Darcy's law predicts widespread forest mortality under climate warming. *Nature Climate Change* 5, 669-672 (2015)

K.E. Trenberth, A. Dai, G. van der Schrier, P.D. Jones, J. Barichivich, K.R. Briffa, J. Sheffield. Global warming and changes in drought. *Nature Climate Change* 4, 17-22 (2014).

Williams A. P. *et al.*, Temperature as a potent driver of regional forest drought stress and tree mortality. *Nature Climate Change* **3**, 292-297 (2013).

DOI: 10.1038/NCLIMATE2873

SI 5: The results shown in Figure 2 are all from the Sevilleta Long Term Ecological Research (LTER) project at the Sevilleta National Wildlife Refuge in central New Mexico, USA (Pangle et al. 2012). Our experimental plots were established on the eastern slope of the Los Pinos Mountains (34˚23´11˝ N, 106˚31´46˝ W) in the northeastern corner of the wildlife refuge at a mean elevation of 1911m. The site is a piñon pine (*Pinus edulis,* Engelm.) and juniper (*Juniperus monosperma* (Engelm.) Sarg.) woodland, with piñon and juniper basal area and canopy coverage that averaged 20.0 m^2 ha^{-1} and 36.7% respectively across the study site. Climate records (20-yr, 1989-2009) from a nearby LTER meteorological station (Cerro Montoso #42; http://sev.lternet.edu/) indicate a mean annual precipitation total of 362.7 mm/yr. The region is strongly influenced by the North American Monsoon, with a large fraction of annual precipitation occurring in July, August, and September. Mean annual temperature (20-yr) at this nearby LTER site was 12.7 ˚C, with a mean July maximum of 31.0 ˚C and a mean December minimum of -3.3 ˚C. In total, our study site consisted of 12 experimental plots located in three replicate blocks that varied in slope %, aspect, and soil depth. A more detailed description and discussion of the vegetative cover and soil properties at this site have been presented elsewhere (see Pangle et al. 2012 and Plaut et al 2012).

The study utilized four different experimental treatments applied in three replicate blocks. The four experimental treatments included 1) un-manipulated, ambient control plots, 2) drought plots, 3) supplemental irrigation plots, and 4) cover-control plots. The three replicated blocks differed in their slope and aspect. One block was located on south facing slopes, one on north facing slopes, and one in a flat area of the landscape. Drought, cover-control, and irrigation infrastructure was installed in 2007, with drought treatments effectively in place by August 2007. The irrigation system was tested in 2007, and supplemental irrigations began in year 2008.

To effectively reduce water availability to trees, we constructed three replicated drought structures that covered an area of 40 m × 40 m (1600 m^2). Each drought plot consisted of 29 parallel troughs running across the 40 m plot, constructed with overlapping 3 ft × 10 ft (0.91 m × 3.05 m) pieces of thermoplastic polymer sheets fixed to horizontal rails that were approximately 1m in height. The plastic sheets were bent into a concave shape to collect and divert the precipitation off plot. The total plastic coverage in each plot is ~45% (± 1%) of the 1600 m^2 plot area, resulting in ~55% of ambient precipitation reaching the ground in drought plots. For an in-depth discussion that compares the severity of our experimentally imposed drought to historical drought conditions observed in the past 100 years, please see Plaut et al. 2013.

In addition, we built cover-control infrastructures to investigate the impact of the plastic drought structures independent of changes in precipitation. The cover-control treatment had the same dimensions as the drought plots, with plastic attached to the rails in a convex orientation so precipitation would fall off the plastic and onto the plot, thus these plots received the same amount of precipitation as un-manipulated ambient plots. Our irrigation system consisted of above-canopy sprinkler nozzles configured to deliver a supplemental rainstorm event of 19 mm (~rate of 19mm hr^{-1}). Our supplemental water was trucked to site and stored in above ground tanks prior to irrigation events. Supplemental irrigations (19 mm $event^{-1}$) were applied throughout the growing season (~ monthly intervals) at an annual rate of 57, 69.5, 112, 107, and 95 mm yr^{-1} from years 2008 thru 2012. At no time did we attempt to alter the timing or the onset of either pre-monsoon or monsoon season precipitation events; our supplemental irrigations were only intended to alleviate plant water stress during the entire frost-free growing season.

Multiple physiological characteristics of ten sample trees (five piñon and five juniper) within each plot were monitored by automated sensors and periodic manual measurements to assess tree responses to precipitation manipulations. Leaf level gas exchange was measured from 2010 through 2012 using standard approaches explained in Limousin et al. (2013). We performed periodic assessments of canopy greenness and canopy dieback (for the same sample trees) during each growing season (across all plots). Accordingly, across all replicate blocks, a total of n=120 trees (n=60 per species) were initially designated and monitored across the 6+ year duration of the study. For each treatment factor, a subset of n=30 monitored trees (n=15 per species) within this group were subjected to each level of precipitation manipulation (i.e., ambient, drought, supplemental irrigation, and cover-control treatment). And, when available within a given experimental plot, extra replacement trees were designated and monitored in place of original sample trees that experienced either mortality or severe canopy dieback over the 6+ yr duration of the experiment.

Predawn (Ψ_{PD}) and mid-day (Ψ_{MD}) plant water potentials were measured with multiple Scholander-type pressure chambers (PMS Instrument Co, Albany, OR) on excised foliage from sample trees (n=10 per plot) throughout the growing season of each year across all plots. Stem sap-flow (J_S) was measured in sample trees (n=10 per plot) using Granier heat dissipation sap flow sensors installed in 2007 in each plot within the south aspect block (plots 9-12). Trees in north facing (plots 5-8) and flat blocks (plots 1-4) were instrumented with sap-flow sensors during the 2009 season, and the south facing block was re-instrumented with new replacement sapflow sensors in year 2010. All sample trees had two 10 mm Granier sap-flow sensors installed in the outermost sapwood (Granier 1987). Each sensor used the traditional two probe heated and unheated reference design (Granier 1987), with two additional probes located 5 cm to the right side of the primary probes to correct for axial temperature gradients in the stem (Goulden and Field 1994). We found that this compensation for axial temperature gradients is critical to reduce measurement noise resulting from the open-canopy and high radiation environment of this ecosystem. In addition, stems were wrapped with reflective insulation (Reflectix Inc., Markleville, IN) in an effort to shield sap-flow probes from short term ambient temperature fluctuations and direct solar irradiance. Sap-flow (J_S) was calculated according to the methods outlined in Granier (1987) and Goulden and Field (1994). Sapwood depth was greater than 10 mm on the majority of instrumented trees, thus only a very small % of measurements across the 2007-2012 period required a correction due to sensor installation in non-functional stem heartwood (see Clearwater et al. 1999). All data from sap-flow sensors was recorded using Campbell Scientific AM16/32 multiplexers and CR1000 dataloggers (Campbell Scientific, Logan, UT). Data processing was performed using Matlab software (R2011a; The Mathworks, Natick, MA, USA).

Plant hydraulic conductance (K_s, units of mol m^{-2} s^{-1} MPa^{-1}) was calculated using the following relationship based on Darcy's law (Wullschleger et al. 1998, Sperry et al. 2002);

$$K_s = E / (\Psi_{PD} - \Psi_{MD}),$$

with E equal to midday J_S (per unit sapwood area) measured from 1100-1400 hours, and Ψ_{PD} and Ψ_{MD} representing soil (Ψ_S) and midday leaf (Ψ_{MD}) water potential respectively. Due to the short stature of our sample trees (mean height = 4.0 m, range 2.2 to 6.3 m), we did not consider or account for height/gravitational effects in our K_s assessments. For calculations of K_s, only measurements with a midday water potential gradient of least 0.5 MPa difference between Ψ_{PD}

DOI: 10.1038/NCLIMATE2873

and Ψ_{MD} ($\Delta\Psi$) were retained in the analysis. The use of a 0.5 MPa $\Delta\Psi$ gradient threshold served to minimize erroneous K_s estimates that would result from the use of small denominator estimates in calculations (i.e., particularly small $\Delta\Psi$ values). Furthermore, a 0.5 MPa $\Delta\Psi$ cut-off served to remove a significant % of periods where stomata were closed at midday due to drought conditions. Thus these estimates are conservative.

Percentage loss of conductance was estimated as the ensemble product of five model simulations: Sperry, MuSICA, TREES, ED(X), and CLM(ED). These simulations were highly tuned using on-site measurements and represent whole-tree hydraulic conductance loss. More details can be found in (*13*).

Leaf samples for starch analysis were collected approximately monthly from all target trees on ambient, irrigation, and drought plots in block three starting in February 2007. Collections began on all target trees in the other two blocks in 2009. In 2009 and 2010, winter collections were excluded and sampling was focused on seasonal changes during the growing season, with collections in spring (March-April), pre-monsoon (May-June), monsoon (July-Sept), and post-monsoon (Oct-Nov) periods. There was no spring collection in 2010. Cover control samples were collected on the first four sampling dates in 2009. These samples did not reveal significant differences in nonstructural carbohydrate (NSC) from ambient samples, and so sampling was discontinued on cover control plots after June 2009. To reduce the number of samples for analysis, samples from trees on non-drought plots (ambient, cover control, irrigation) and the drought plot in block one (because no trees on the plot had died as of the 2011 growing season) were pooled by plot, species, tissue, and date. This pooling reduced sample number on these plots from 5 to 1 within a given plot, species, tissue and date. The only non-pooled samples were from drought plots in blocks two and three. When trees died (defined as 100% foliar browning; Gaylord et al. 2013) they were excluded from the collection protocol. Piñon sampling was discontinued in August 2009 after the last of the drought trees in blocks two and three had died. Foliar starch was analyzed following the protocol described by Hoch et al. (2002), with minor modifications. All samples were covered in dry ice immediately after collection and stored at -70 °C after transport to the lab. Samples were microwaved at 800 watts for 5 minutes to stop enzymatic activity, then dried at 65 °C for 48 hours and ball-milled to a fine powder (High Throughput Homogenizer, VWR). Samples that were pooled to reduce the number of samples for analysis were thoroughly homogenized after milling. Approximately 12 mg of fine ground leaf material was extracted in a 2mL deep-well plate with 1.6 mL distilled water for 60 minutes in a 100 °C water bath (Isotemp 105, Fisher Scientific). Following extraction, an NAD-linked enzymatic assay was used to evaluate NSC content. NSCs are defined here as free, low molecular weight sugars (glucose, fructose, and sucrose), plus starch. All NSCs were hydrolysed to glucose, linked to the reduction of NAD+ to NADH, and monitored at 340 nm with a spectrophotometer (Cary 50 UV-Vis). Starch was calculated as NSC minus low molecular weight sugars. All NSC content values are expressed as percent of dry matter.

Clearwater, Michael J., Frederick C. Meinzer, José Luis Andrade, Guillermo Goldstein, and N. Michelle Holbrook. Potential errors in measurement of nonuniform sap flow using heat dissipation probes. *Tree Physiology* **19**, no. 10: 681-687. (1999)

Goulden, M. L., and C. B. Field. Three methods for monitoring the gas exchange of individual tree canopies: ventilated-chamber, sap-flow and Penman-Monteith measurements on evergreen oaks. *Functional Ecology*: 125-135. (1994)

Granier, A. Evaluation of transpiration in a Douglas-fir stand by means of sap flow measurements. *Tree Physiology* **3**, no. 4: 309-320. (1987)

Hoch, G., Popp, M. Körner, C. Altitudinal increase of mobile carbon pools in Pinus cembra suggests sink limitation of growth at the Swiss treeline. *Oikos* **98**: 361–374. (2002)

McDowell, Nate G., Rosie A. Fisher, Chonggang Xu, J. C. Domec, Teemu Hölttä, D. Scott Mackay, John S. Sperry et al. Evaluating theories of drought-induced vegetation mortality using a multimodel–experiment framework. *New Phytologist* **200**, no. 2: 304-321. (2013)

Pangle RE, Hill JP, Plaut JA, Yepez EA, Elliot JR, Gehres N, McDowell NG, Pockman WT. Methodology and performance of a rainfall manipulation experiment in piñon-juniper woodland. *Ecosphere* **3**: art28. (2012).

Wullschleger, Stan D., F. C. Meinzer, R. A. Vertessy. A review of whole-plant water use studies in trees. *Tree Physiology* **18**, no. 8-9: 499-512. (1998)

Sperry, J. S., U. G. Hacke, R. Oren, and J. P. Comstock. "Water deficits and hydraulic limits to leaf water supply." *Plant, Cell & Environment* **25**, no. 2: 251-263. (2002)

DOI: 10.1038/NCLIMATE2873

SI Figure S1: Long-term water potential record and interpretation.

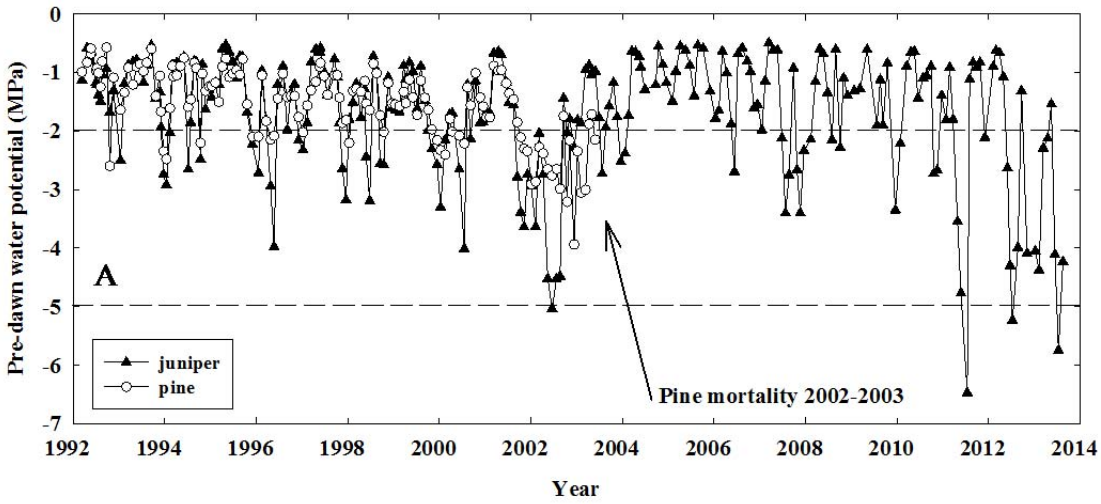

SI Figure S1A) A 21–year time series of monthly pre-dawn Ψ of piñon pine and juniper in Los Alamos, New Mexico, extending prior time series[22,23]. Piñon trees died in 2002-03, with surviving juniper trees becoming the dominants. The species-specific Ψ_{A0} values are presented as horizontal dashed lines. **B)** Dying juniper trees in northern New Mexico in 2013, photo courtesy Mark Watson.

The water potential data shown in SI Figure 1A was collected on a minimum of five trees for pine and another five for juniper (often we sampled around 10 trees each). The methods were identical to those described for the Sevilleta plot (SI 4), except we sample two twigs per tree rather than just one, and average the within tree values. Canopy loss and mortality was observed weekly during the drought events at both sites[21,23]. In pine trees, the entire canopy turns from green to orange within a few weeks, with litterfall happening immediately thereafter.

D rises exponentially with temperature, thus chronic temperature rise is forcing a particularly rapid rise in D^{20} with implications for Ψ, G_s and survival (equation 1 and Fig. 1B). To ascertain the likelihood of future mortality, we first determined if climate parameters predicted from the Coupled Model Intercomparison Project (CMIP5) multi-model ensembles such as precipitation and *D* could be used to infer our long-term Ψ_{pd} observations (1992-2013). Using the dataset from the long-term monitoring site (SI Fig. 1A) we found annual precipitation and annual mean *D* together explain 70 and 80% of the annual variation in growing-season mean Ψ_{pd} for pine and juniper, respectively (SI Fig. 2). An independent test against the drought manipulation site (Fig. 2) also gave a strong predictive relationship for both species (SI Fig. 2). The final relationship using both field sites is:

pine Ψ_{pd} (april-august) = -10^ [0.993-0.455•log10(ppt)+0.028•*D*] (2),
juniper Ψ_{pd} (april-august)=-10^[1.461-0.724•log10(ppt)+0.059•*D*] (3),

in which annual precipitation (ppt, mm) and *D* (hPa) are total and average, respectively. Equations (2,3) are extremely similar to that used to predict tree ring growth[20], suggesting growth and Ψ_{pd} are coupled and that these variables are broadly applicable.

SI 6: Regressions for Figure 2.
Figure 2B pine: $G_s = 0.345e^{1.66\Psi pd}$, r^2=0.79
Figure 2B juniper: $G_s = 0.162e^{0.51\Psi pd}$, r^2=0.80

Figure 2C pine: photosynthesis = $2.82*\Psi_{pd}$ +7.4, r^2=0.66
Figure 2C juniper: photosynthesis = $1.287*\Psi_{pd}$ +7.9, r^2=0.74

Figure 2D pine: PLC = $-20.23*\Psi_{pd}$ + 1.80, r^2=0.46
Figure 2D juniper: PLC = $-6.42*\Psi_{pd}$ - 0.20, r^2=0.69

Figure 2E pine: hydraulic conductance = $0.83e^{0.30\Psi pd}$, r^2=0.21
Figure 2E juniper: hydraulic conductance = $1.01e^{0.36\Psi pd}$, r^2=0.36

Figure 2F pine: NSC = $1.44*\Psi_{pd}$ + 6.45, r^2=0.14
Figure 2F juniper: NSC = $0.62*\Psi_{pd}$ + 7.21, r^2=0.06

SI 7: Foliar starch has proven a robust indicator of the carbon starvation process in piñon pine (Adams et al. 2013; McDowell et al. 2013; Sevanto et al. 2014; Dickman et al. 2014), and redwood (Quirk et al. 2013) but may underestimate the process in some conifers (e.g. Hartmann et al. 2013).

H.D. Adams, *et al*. 2013. Nonstructural leaf carbohydrate dynamics of *Pinus edulis* during drought-induced tree mortality reveal role of carbon metabolism in mortality mechanism. *New Phytologist* 197: 1142-1151.

DOI: 10.1038/NCLIMATE2873

H. Hartmann, Trumbore, S. and Ziegler, W. (2013) Lethal drought leads to reduction in nonstructural carbohydrates (NSC) in Norway spruce tree roots but not in the canopy. Functional Ecology 27: 413-427.

L.T. Dickman, N.G. McDowell, S. Sevanto, R.E. Pangle, W.T. Pockman. 2014. Carbohydrate dynamics and mortality in a piñon-juniper woodland under three future precipitation scenarios *Plant, Cell and Environment,* DOI: 10.1111/pce.12441.

N.G. McDowell, Fisher RA, Xu C, Domec JC, Hölttä T, Mackay DS, Sperry JS, Boutz A, Dickman L, Gehres N, Limousin JM, Macalady A, Martinez-Vilálta J, Mencuccini M, Plaut JA, Ogee J, Pangle RE, Rasse DP, Ryan MG, Sevanto S, Waring RH, Williams AP, Yepez EA, Pockman WT. 2013. Evaluating theories of drought-induced vegetation mortality using a multi-model-experiment framework. *New Phytologist* 200(2), 304-321

S. Sevanto, McDowell NG, Dickman LT, Pangle R, Pockman WT. 2013. How do trees die? A test of the hydraulic failure and carbon starvation hypotheses. *Plant, Cell and Environment,* doi: 10.1111/pce.12141

J. Quirk, N.G. McDowell, J.R. Leake, P.J. Hudson, D.J. Beerling. Carbon dioxide starvation, drought, and Cenozoic forest retreat. 2013. *American Journal of Botany,* 100: 582-591.

SI Figure S2: Evaluation of model predictions of predawn water potential

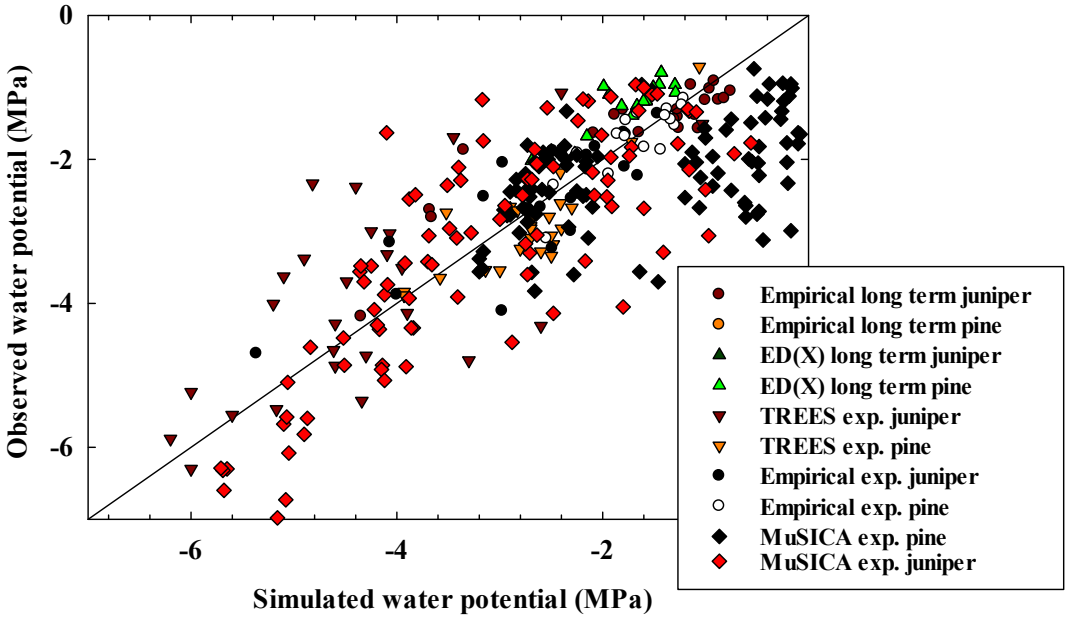

SI Figure 2) Predictions of April through August mean Ψ versus observed Ψ for the long-term (21 year) observations as well as the drought manipulation study for juniper and piñon pine. For pine and juniper, respectively, the empirical water potential approach yielded r^2 values of 0.70 and 0.77, ED(X) simulation yielded r^2 values of 0.82 and 0.77, TREES simulation yielded r^2 values of 0.69 and 0.68, and MuSICA simulation yielded r^2 values of 0.24 and 0.73.

Annual growing-season Ψ_{pd} records were developed for each species at the experimental (Sevilleta, SI 4) and long-term observational (Los Alamos, Fig. S1) sites. At the experimental site, a record was developed for each precipitation treatment. Ψ_{pd} measurements were made approximately once per month, generally toward the end of the month. Growing-season records were then calculated by averaging across April–August values. These records covered 1992–2013 at the Los Alamos site and 2007–2013 at the Sevilleta site. For each species, we related the Ψ_{pd} records to seasonal climate data. Based on a priori knowledge of climate responses in the region[20], we developed multivariate equations that estimated growing-season Ψ_{pd} from annual (previous September through growing-season August) precipitation total and mean vapor-pressure deficit (D). We elected to use annual rather than seasonal climate data to avoid over-fitting the multivariate equations. Notably, annually averaged D is dominated by variability in the warm-season, which is when the ecological influence of D variability appears to be strongest in the region[20].

DOI: 10.1038/NCLIMATE2873

SI 8: Model-specific developments and application

Table S1: A summary of how empirical variables were utilized or simulated by models. The model input parameters are typically static (e.g. soil texture), model driver parameters typically change over time (e.g. micrometeorological data), and model output represents simulated variables. See [13] for more details.

Variable	TREES	MuSICA	ED(X)
Mortality	n/a	n/a	Output
LAI	Input	Input	Output
Density	n/a	Input	Input
Height	Input	Input	Input
Cover	n/a	n/a	Output
NSC	Output	Output	Output
SLA	Input	Input	Input
Ψ_{pd}, Ψ_{md}	In/Output[1]	Output	Output
E[2]	In/Output[1]	Output	Output
Respiration	Output	In/Output	n/a
Vcmax	Input	Input	Input
Vulnerability	Input	Input	Input
Ψ_{soil}	Output	Output	Output
SWC	Output	Output	n/a
Soil depth	Input	Input	Input
Soil temp.	Input	Output	n/a
Soil texture	Input	Input	Input
Allometry	Input	Input	Input
Air temp.	Driver	Driver	Input
VPD	Driver	Driver	Input
PAR	Driver	Driver	Input
Wind speed	Driver	Driver	Input
Atm Press.	Driver	Driver	Input
Hyd Cond	Output	Output	Input

[1] Ψ_{pd}, Ψ_{md}, and E at saturated hydraulic conductance (K) input; values at other times output
[2] Used for evaluation of all models

Model specific developments and application

TREES: The Terrestrial Regional Ecosystem Exchange Simulator (TREES) (Samanta *et al*., 2007; Loranty *et al*., 2010; Mackay *et al*., 2012; Roberts 2012) is a dynamic model of plant water and carbon flows. A unique methodological improvement in TREES is a full coupling of the Sperry *et al*. (1998) model of plant water balance and cavitation with stomatal conductance (G_S), photosynthesis (A), and E driven by energy supply and vapor demand. Thus, TREES explicitly incorporates A and dynamic plant hydraulic conductance into a unified numerical solution. It also predicts *PLC*, *NSC*, growth efficiency, and carbon allocation to leaves, roots, and stem. The model was calibrated using pre-drought gas exchange, transpiration, water potentials,

and vulnerability curve measurements (Plaut *et al*., 2012, Limousin *et al*., 2013). Root-to-leaf area (RL) ratios for each species were optimized to maximize carbon uptake for a given amount of water loss, a conservative approach that is appropriate for the dry Southwest climates. This analysis predicted an optimal root RL of 2 for pine and 3 for juniper. TREES was set up to re-adjust the plant hydraulic conductance once per year, in early spring (on year-day 60), to account for refilling. The rooting zone had a maximum depth in the shallow simulations of 19cm, and a maximum depth in the deep simulations of 89cm. Soil water balance was updated in each half-hour time step for each layer using precipitation inputs, drainage, and rhizosphere fluxes. Water potentials, hydraulic conductances, and fluxes were calculated based on the updated soil moisture, cavitation status, and transpiration demand. Allocation of carbon to leaves was allowed to adjust upward based on available NSC and downward with increasing PLC. Root area was recomputed annually using the updated leaf area and the pre-set optimal RL.

MuSICA: The MuSICA model is a multilayer, multi-leaf process-based biosphere-atmosphere gas exchange model that simulates the exchanges of mass (water, CO_2) and energy in the soil-vegetation-atmosphere continuum (Ogée *et al*., 2003). The version of the model used in this study includes a more detailed description of root water uptake and plant water storage dynamics, as well as soil water hydraulic redistribution and root cavitation (Domec *et al*., 2012; McDowell et al. 2013) and plant *NSC* storage dynamics (Ogée *et al*., 2009; McDowell et al. 2013). Stand density, biomass, leaf area, and soil properties were taken from Pangle *et al*. (2012) and Plaut *et al*. (2012). The model was calibrated using pre-drought gas exchange and photosynthetic parameters, stomatal response to water potentials and vulnerability curve measurements (Plaut *et al*., 2012, Limousin *et al*., 2013). Maximum rooting depth and root distribution for both species were taken from Plaut et al. (2012). Both species were modeled at the same time and thus competed for the same soil water.

To evaluate the model performance we forced the MuSICA model with meteorological values (radiation, wind speed, temperature, humidity, precipitation) collected at the site and quantified its ability to reproduce midday and predawn leaf water potentials and daily tree transpiration measured on each species between 2007 and 2011 (e.g., see SOM Fig. 2).

For the simulations shown in the main text, we forced MuSICA with two CMIP5 climate scenarios (see main text) assuming either shallow or deep rooting depths for both species, and all other parameters being equal. Mortality rates for each species were computed as with the other models, using predawn leaf water potential predictions from MuSICA over the four simulations (2 climate scenarios $\times$ 2 rooting depths).

ED(X): The Ecosystem Demography (ED) model tracks cohorts of trees based on their sizes (Moorcroft *et al*., 2001). ED(X) simulates tree mortality of cohorts based on the assumption of carbon starvation (Fisher *et al*., 2010) and hydraulic failure (Xu *et al.* 2013). To better present the seasonal cycles of carbon storage, instead of using *GPP* directly for growth, it is first all fed into the *NSC* pool, which is then used by respiration and growth of new tissue determined by carbon sink strength (*13*). Plant hydraulics and hydraulic failure are simulated using existing theories on plant water storage (Meinzer *et al.* 2003) and hydraulic conductivity (Sperry *et al.* 1998). Specifically, the model simulates water storage in tree xylem, which declines during drought due to leaf and root water loss. The reduced water content can lead to cavitation (forming of bubbles in xylem conduits), which impairs the xylem conductivity (Sperry 2000). If

the amount of cavitation passes a critical threshold, xylem becomes dysfunctional and hydraulic failure ensues (Urli *et al.* 2013). The model is first tuned to fit the Sevilleta data of predawn leaf water potential. Then it is applied for the independent long-term observation site at Los Alamos shown in SI Fig. 1A for model evaluation, with different soil depth and texture.

Domec J-C, Ogée J, Noormets A, Jouangy J, Gavazzi M, Treasure E, Sun G, McNulty S, King JS. Interactive effects of nocturnal transpiration and climate change on the root hydraulic redistribution and carbon and water budgets of Southern US pine plantations. *Tree Physiology* **32**: 707-723. (2012)

Fisher R, McDowell N, Purves D, Moorcroft P, Sitch S, Cox P, Huntingford C, Meir P, Woodward FI. Assessing uncertainties in a second-generation dynamic vegetation model caused by ecological scale limitations. *New Phytologist* **187**: 666-681. (2010)

Limousin JM, Bickford CP, Dickman LT, Pangle RE, Hudson PJ, Boutz AL, Gehres N, Osuna JL, Pockman WT, McDowell NG. Regulation and acclimation of leaf gas-exchange in a piñon-juniper woodland exposed to three different precipitation regimes. *Plant, Cell & Environment,* DOI: 10.1111/pce.12089. (2013)

Loranty MM, Mackay DS, Ewers BE, Traver E, Kruger EL. Competition for light between individual trees lowers reference canopy stomatal conductance: results from a model. *Journal of Geophysical Research - Biogeosciences* **115**: G04019, doi:10.1029/2010JG001377 (2010).

Mackay DS, Ewers BE, Loranty MM, Kruger EL, Samanta S. Bayesian analysis of canopy transpiration models: A test of posterior parameter means against measurements. *Journal of Hydrology* **432-433**: 75-83 (2012)

McDowell, Nate G., Rosie A. Fisher, Chonggang Xu, J. C. Domec, Teemu Hölttä, D. Scott Mackay, John S. Sperry et al. Evaluating theories of drought-induced vegetation mortality using a multimodel–experiment framework. *New Phytologist* 200, no. **2**: 304-321. (2013)

Meinzer, F. C.; James, S. A.; Goldstein, G.; Woodruff, D., Whole-tree water transport scales with sapwood capacitance in tropical forest canopy trees. *Plant Cell Environ*, **26**(7), 1147-1155. (2003)

Moorcroft PR, Hurtt GC, Pacala SW. A method for scaling vegetation dynamics: the ecosystem demography model (ED). *Ecological Monographs* **71**: 557-585. (2001)

Ogée J, Brunet Y, Loustau D, Berbigier P, Delzon S. MuSICA, a CO_2, water and energy multi-layer, multi-leaf pine forest model: evaluation from hourly to yearly time scales and sensitivity analysis. *Global Change Biology* **9**: 697–717. (2003)

Ogée J, Barbour MM, Wingate L, Bert D, Bosc A, Stievenard M, Lambrot C, Pierre M, Bariac T, Loustau D *et al*. A single-substrate model to interpret intra-annual stable isotope signals in tree-ring cellulose. *Plant, Cell & Environment* **32**: 1071-1090. (2009)

Pangle RE, Hill JP, Plaut JA, Yepez EA, Elliot JR, Gehres N, McDowell NG, Pockman WT. Methodology and performance of a rainfall manipulation experiment in piñon-juniper woodland. *Ecosphere* **3**: art28. (2012)

Plaut JA, Yepez EA, Hill J, Pangle R, Sperry JS, Pockman WT, McDowell NG. Hydraulic limits preceding mortality in a piñon-juniper woodland under experimental drought. *Plant, Cell and Environment* **35**: 1601-1617. (2012)

Roberts. *Development of a coupled ecosystem exchange plant hydraulic model to explore drought related plant mortality*. Master Thesis, University at Buffalo, Buffalo, NY, USA. (2012)

Samanta S., Mackay DS, Clayton M, Kruger EL, Ewers BE. Bayesian analysis for uncertainty estimation of a canopy transpiration model. *Water Resources Research* **43**: W04424, doi:10.1029/2006WR005028. (2007)

Sperry JS, Adler FR, Campbell GS, Comstock JP. Limitation of plant water use by rhizosphere and xylem conductance: results from a model. *Plant Cell & Environment* **21**: 347-359. (1998)

Sperry, J. S., Hydraulic constraints on plant gas exchange. *Agric For Meteorol***, 104**, (1), 13-23. (2000)

Urli, M.; Porté, A. J.; Cochard, H.; Guengant, Y.; Burlett, R.; Delzon, S., Xylem embolism threshold for catastrophic hydraulic failure in angiosperm trees. *Tree Physiol***,** *10.1093/treephys/tpt030*. (2013)

Xu, Chonggang, Nate G. McDowell, Sanna Sevanto, and Rosie A. Fisher. Our limited ability to predict vegetation dynamics under water stress. *New Phytologist* **200**, no. 2: 298-300. (2013)

Detailed model descriptions:

TREES: The Terrestrial Regional Ecosystem Exchange Simulator (TREES) (Mackay *et al*., 2003; Samanta *et al*., 2007; Loranty *et al*., 2010; Mackay *et al*., 2012) that operates as a physiology model at the scale of individual trees or as an ecosystem model for whole stands. At the plant scale the model couples photosynthesis, stomatal conductance, and transpiration in a steady state solution for sun and shade canopy at 30-minute time steps, and forced with micrometeorological data (air temperature, wind speed, radiation, vapor pressure deficit, and soil temperature). This coupled canopy model and the plant water balance model (Sperry *et al*., 1998) were combined into a single, integrated model to explicitly simulate soil-plant hydraulics and hydraulic failure, and to provide both demand and supply limits on stomatal control of carbon uptake and water loss (Roberts, 2012), as well as carbon utilization and allocation.

At the whole plant canopy scale stomatal conductance (G_S) was calculated by combining Darcy's Law and Fick's law of diffusion as

$$G_S = K_L (\Psi_S - \Psi_L)/D \quad (1)$$

where $K_L(\Psi)$ and Ψ_L are whole-plant hydraulic conductivity and leaf water potential, respectively; D is vapor pressure deficit in the canopy; and Ψ_S is soil water potential integrated over the rooting depth of the plant. The canopy and plant water balance model components are solved iteratively until they converge on a transpiration rate, with simultaneous solution of photosynthesis and stomatal conductance. For this study TREES discretized each modeled tree into three root modules, each having an absorbing and conducting element, and one canopy module having a conducting element and a lateral element with sun and shade sub-elements for gas exchange. The rhizosphere around each absorbing root element was discretized into five sub-

DOI: 10.1038/NCLIMATE2873

elements for transporting water between the bulk soil and the absorbing root (see Sperry *et al.*, 1998 for details). The root zone soil water balance was maintained by the model and updated, in separate layers defined by discrete root depth, using rhizosphere flux rates determined as part of the plant water balance model solution. The model moves water at the soil-root interface either from soil to root or from root to soil as a function of the pressure gradients. Once the plant hydraulic solution converges the photosynthetic assimilation is accumulated and for daily updating of NSC.

Plant mortality due to hydraulic failure can be predicted using TREES because of cavitation. Plant mortality due to carbon starvation is not explicitly modeled. However, changes in NSC are simulated as the difference in carbon uptake and utilization. A reduction in carbon uptake occurs when stomatal closure reduces photosynthetic assimilation of carbon. Using hydraulic conductance as a proxy for carbon transport reduces carbon utilization. Consequently, as a simulated tree approaches a condition that suggests that it would be susceptible to mortality due to stomatal closure and reduced water for carbon transport, both carbon uptake and utilization decline, which means the rate of change of NSC can be negligible. Although this would not directly predict mortality due to carbon starvation a combination of plant hydraulic conductivity, hydraulic safety, cavitation, changes in NSC, carbon uptake, and carbon use collectively can be used to diagnose the health status of a simulated tree.

Changes in NSC for the whole plant were calculated at daily time steps as

$$dC_{NS}/dt = C_A - C_G - C_M \quad (2)$$

where C_{NS} is NSC, C_A is photosynthetically assimilated carbon for period t (*i.e.* 1 day), C_G is growth and growth respiration allocated in time t, and C_M is maintenance respiration over period t. Carbon is allocated first to C_M and then to C_G. C_M was calculated using separate temperate-based respiration rates for leaf, stem, and roots as

$$C_M = (R_{root}\, C_{root}\, r^{Troot} + R_{stem}\, C_{stem}\, r^{Tstem}\, e^{0.67*\log(10C_{stem})}/10 + R_{leaf}\, C_{leaf}\, r^{Tleaf})\, f_{M\sim K} \quad (3)$$

where R terms refer to root, stem, and leaf intrinsic respiration rates (fraction), C terms are carbon pools, T terms are temperatures, r is a respiration coefficient, and $f_{M\sim K}$ is a function that reduces the transport of NSC to sites for maintenance respiration as a function of hydraulic conductivity and saturated hydraulic conductivity K_{Lsat} as

$$F_{M\sim K} = K_L(\Psi)/K_{Lsat} \quad (4)$$

When root temperature is at least 5 ºC, then C_G is calculated as a parameterized fraction (β_G) of C_A as

$$C_G = \beta_G C_A f_{G\sim K} \quad (5)$$

where $f_{G\sim K}$ is function that reduces the transport of NSC to sites for growth as a function of hydraulic conductivity and saturated hydraulic conductivity K_{Lsat} as

$$f_{G\sim K} = [K_L(\Psi)/K_{Lsat}]^2 \quad (6)$$

TREES was parameterized and run on individual trees using individual tree data to the extent possible. The model was tuned to each tree using species-specific allometric equations and the basal area of each respective tree, and sap flux data for each respective tree. TREES carbon pools were initialized for each individual tree using allometric equations for the root, stem, and leaf structural carbon pools and measured NSC (McDowell *et al.*, *unpublished data*). TREES was parameterized for hydraulics by species using vulnerability to cavitation curves (Plaut *et al*., 2012), and by individual tree using sap flux data to obtain midday transpiration at saturated hydraulic conductivity. Measured pre-dawn and mid-day water potentials at saturated hydraulic conductivity were also used. Site-specific soil texture data was used to parameterize the soil hydraulic properties. The photosynthesis routines were parameterized using species and treatment specific data collected in the study. All canopy calculations were expressed on a per unit leaf area basis, and so leaf area index by individual tree was obtained from allometry and taking the calculated total leaf area divided by projected crown area (Loranty *et al*., 2010; Mackay *et al*., 2010). We assumed that each tree operated independently of its neighbors, and so there were no interactions between root uptake rate among trees. The trajectory of carbon and water pools and fluxes for each tree was therefore independently calculated, and determined as a function of each respective tree's carbon pools, hydraulic properties, and effect on its local soil water conditions.

MUSICA: The multilayer, multi-leaf, process-based biosphere-atmosphere gas exchange model MuSICA has been primarily developed to simulate the exchanges of mass (water, CO_2) and energy in the soil-vegetation-atmosphere continuum and is particularly well designed for studies on conifer trees because it deals with needle clumping of various needles cohorts (Ogée *et al*., 2003). MuSICA assumes the terrain to be relatively flat and the vegetation horizontally homogeneous. Several species can share a common soil and the mixed canopy is partitioned into several vegetation layers (typically 10-15) where several leaf types (sunlit/shaded, wet/dry) for each cohort and species are distinguished. Stand structure is therefore explicitly accounted for and competition for light and water between species can be explored. The version of MuSICA used in this study is the same as in other studies (e.g. Domec *et al*., 2012; McDowell et al. 2013). It typically produces output at a 30-min time step and can be run over multiple years or decades as long as the vegetation structure is given. A brief overview of the different sub-models embedded in this MuSICA version is given below.

DOI: 10.1038/NCLIMATE2873

The radiative transfer scheme is based on the radiosity method and supports multiple (broad-leaf or needle-leaf) species in a given vegetation layer (Sinoquet *et al*., 2001). Rain interception and canopy evaporation are computed for each species and vegetation layer using the concept of maximum storage capacity (Rutter et al. 1971). Vertical profiles of the microclimate (air temperature, humidity and CO_2) within the vegetation canopy are computed using the Lagrangian near-field theory (Raupach 1988). A multilayer, coupled heat and water soil transport model that explicitly accounts for root water uptake for each species is also implemented. Water storage in the plants is accounted for using a single water storage capacity for each species that scales with leaf area (Williams *et al*., 2001). The soil water retention curve and the unsaturated soil hydraulic conductivity are described according to the model of Van Genutchen (1980). The leaf-to-air energy, water and CO_2 exchange model consists of a photosynthesis model (Farquhar *et al*., 1980), a stomatal conductance model (Leuning, 1995), a leaf boundary-layer model (Nikolov *et al*., 1995) and a leaf energy budget equation. Species-specific photosynthetic parameters are the maximum rates of carboxylation and electron transport, mitochondrial respiration and quantum yield. All these parameters vary with leaf temperature and/or leaf ontogeny and are thus prescribed at a given temperature (25°C) and for young and old leaves or needles. Day respiration is computed using the night respiration rate parameterization and a light inhibition factor. Woody respiration is scaled using living biomass, basal respiration rates and Q_{10} values and is assumed to depend on air temperature only. Soil and litter respiration rates are a function of soil temperature and soil moisture. Soil water deficit affects the maximum stomatal conductance and photosynthetic capacity and is described by a sigmoid curve of leaf water potential, with a common threshold and slope for both variables. Soil water deficit also induces root cavitation that is described by Weibull-like curves of plant water potential (Domec & Gartner 2001).

The parameterisation of the model was done as follows. Stand density, woody biomass, leaf area, and soil properties were taken from Pangle *et al*. (2012) and Plaut *et al*. (2012). Maximum rooting depth and root-to-shoot area ratios were taken from Plaut et al. (2012). Living tissue respiration was parameterized using basal respiration rates determined at the site (McDowell et al. 2013). Soil and litter respiration rates were parameterized from soil respiration data collected at the site in 2006 and 2007 (White, 2008). Stomatal conductance and photosynthetic parameters (maximum rates of carboxylation, rate of photosynthetic electron transport and mesophyll conductance) were taken from Limousin et al (2013).

To evaluate the model performance we forced the MuSICA model with meteorological values (radiation, wind speed, temperature, humidity, precipitation) collected at the site and quantified its ability to reproduce midday and predawn leaf water potentials and daily tree transpiration measured on each species between 2007 and 2011 (e.g., see SOM Fig. 2).

For the simulations shown in the main text, we forced MuSICA with two CMIP5 climate scenarios (see main text) assuming either shallow or deep rooting depths for both species, and all other parameters being equal. Mortality rates for each species were computed as with the other models, using predawn leaf water potential predictions from MuSICA over the four simulations (2 climate scenarios × 2 rooting depths).

Dewar RC, Medlyn BE, McMurtrie RE. A mechanistic analysis of light and carbon use efficiencies. Plant, Cell and Environment , **21**: 573–588 (1998).

Domec JC, Gartner BL (2001) Cavitation and water storage capacity in bole xylem segments of mature and young Douglas-fir trees. *Trees*, **15**: 204–214 (2001).

Farquhar, G.D., S. von Caemmerer and J.A. Berry. A biochemical model of photosynthetic CO2 assimilation in leaves of C3 species. Planta **149**, 78–90 (1980).

Leuning, R. A critical appraisal of a combined stomatal-photosynthesis model for C3 plants. Plant Cell Environ. **18**:339–356 (1995).

McDowell, Nate G., Rosie A. Fisher, Chonggang Xu, J. C. Domec, Teemu Hölttä, D. Scott Mackay, John S. Sperry et al. Evaluating theories of drought-induced vegetation mortality using a multimodel–experiment framework. *New Phytologist* 200, no. **2**: 304-321 (2013).

Sinoquet H, Le Roux X, Adam B, Ameglio T, Daudet F. RATP: a model for simulating the spatial distribution of radiation absorption, transpiration and photosynthesis within canopies: application to an isolated tree crown. *Plant Cell Environ*., **24**: 395–406 (2001).

Williams, M., E.B. Rastetter, G.R. Shaver, J.E. Hobbie, E. Carpino B.L. Kwiatkowski. Primary production in an arctic watershed; an uncertainty analysis. Ecol. Appli. **11**: 1800-1816 (2001).

Wingate, L., Oǵee, J., Burlett, R., Bosc, A., Devaux, M., Grace, J., Loustau, D., and Gessler, A. Photosynthetic carbon isotope discrimination and its relationship to the carbon isotope signals of stem, soil and ecosystem respiration, New Phytol., **188**, 576–589 (2010).

ED(X): ED(X) generated the most conservative forecasts, with the likelihood of pine mortality approaching 100% (for the average grid cell) by 2078 and only 31% likelihood of juniper mortality by 2100. We used the Ecosystem Demography (ED) model (Moorcroft *et al*., 2001) with modifications described by Fisher *et al*. (2010), McDowell et al (2013) and Xu et al (2013). The model simulates a water storage pool for the plants and calculates the xylem water potential changes based on the relative water content in xylem (Barnard et al 2011). For each 30-minutes time step, the model simulates leaf water potential based on the water balance, which is calculated as the difference between water supply as determined by the Ball-Berry stomata conductance and vapor pressure gradient from leaf to air, and the water demand as determined by the xylem conductance, tree height and the difference between leaf water potential and xylem water potential. The water storage pool is recharged by the root water uptake as determined by the pressure gradient from soil to xylem and the xylem conductance. During the drought, the plant halts photosynthesis if the xylem water potential is lower than minimum leaf water potential with no water recharge from the soil and the water storage will decline due to the loss of water by cuticular transpiration and the root water loss to soil. Regeneration processes were turned off in our simulations because we were focused on the mortality patterns. ED(X) generated the most conservative forecasts in Figure (3), with the likelihood of pine mortality approaching 100% (for the average grid cell) by 2078 and only 31% likelihood of juniper mortality by 2100.

This ED version uses a single soil layer. The soil water potential (ψ_s) is simulated based on an empirical equation as follows (Niu and Yang 2006):

DOI: 10.1038/NCLIMATE2873

$\psi_s = \psi_{s0}\theta^{-\lambda}$ where ψ_{s0} is the reference soil water potential for saturated soil, θ is the volumetric saturation of water in soil pores, and λ is the exponent determined by soil texture, as follows:

$$\lambda = 2.91 + 0.159\mathrm{P}_{\mathrm{clay}},$$

where $\mathrm{P}_{\mathrm{clay}}$ is the percent of clay in the soil.

The maximum plant water supply is calculated based on the water potential gradient between leaf and xylem and xylem resistance as follows:

$$W_{\mathrm{supp}} = \frac{\psi_x - \psi_{l\min}}{r_c R_x / A_s + R_l}$$

where the denominator represents the water transport resistance from trunk to leaf assuming the transport distance is the tree crown radius. Specifically, R_x is the resistance of water transport in xylem ($\mathrm{m}^3\cdot\mathrm{Mpa}\cdot\mathrm{s}/\mathrm{kg}$) with A_s representing the sap wood area (m^2). R_l is the resistance of water transport from branch to leaf ($\mathrm{m}^3\cdot\mathrm{Mpa}\cdot\mathrm{s}/\mathrm{kg}$) and r_c is the crown radius (m).

The xylem conductivity ($\frac{1}{R_x}$) may reduce due to xylem cavitation (Sperry *et al.*, 1998). The proportion loss of conductivity (PLC) is calculated based on the xylem water potential using the Weibull equation as follows (Neufeld *et al.*, 1992):

$$PLC = 1.0 - e^{-(\psi_x/\Phi_{73})^c},$$

where Φ_{73} is the critical soil water potential that cause 73% loss of xylem conductivity and c is the shape parameter for conductivity loss.

The water demand of each leaf layer for a cohort is calculated based on the stomata conductance and relative humidity. Specifically,

$$W_{dem} = \frac{18.0}{r_b + r_s}\frac{(e_s - e_a)}{RT},$$

where r_b and r_s are the boundary layer and stomata resistance of water (*s/m*). R is the gas constant (8, 314 *J/K/kmole*) and *T* is the air temperature (*K*). e_s and e_a are the vapor pressure inside leaf and of the canopy air (*Pa*). r_s is calculated based on the empirical Ball-Berry model (Ball *et al.*, 1987). Specifically,

$$r_s = \frac{1}{C_f}\left(m\frac{A}{C_a}\frac{e_a}{e_s}P_{atm} + 2000\right),$$

where C_a is the CO_2 partial pressure in the canopy air and P_{atm} is the atmospheric pressure (Pa). C_f is the conversion factor from *s/m* to $s \cdot m2 / umol$,

$$C_f = \frac{P_{atm}}{RT}10^9 .$$

The xylem water potential is calculated based on the relative water content as follows (Barnard et al 2011):

$$\psi_x = \frac{a(1-RWC)}{1+b(1-RWC)},$$

where RWC is the relative xylem water content.

The xylem water content changes resulting from the balance of xylem water recharge and water loss from root and leaf. The xylem water recharge rate (kg water/s) is calculated based on the water pressure gradient from soil to xylem and the xylem resistance (R_x, $m^3 \cdot Mpa \cdot s/$ kg water) and the soil-root resistance (R_{rs}, $s \cdot MPa/m$),

$$W_{recharge} = \frac{\psi_s - \psi_x + 9.8h/1000}{hR_x / A_s + R_{rs}},$$

where ψ_s is the soil water potential (*MPa*) and *h* is the height of tree (m). If the soil water potential is less than xylem water potential during drought, the xylem water reduces with root and leaf water loss. The root water loss (*kg water/s*) is calculated based on the water potential gradient from root to soil as follows:

$$W_{rloss} = g_r \max(\psi_x - \psi_s, \psi_{sr\_\max}),$$

where g_r is the root water loss rate (*m/s/Mpa*) and the $\psi_{sr\_\max}$ is the maximum water potential gradient between soil and root due to potential isolation of root from soil under very dry conditions (Tardieu and Simonneau 1997). When the xylem water potential become less than prescribed minimum leaf water potential, the stomata closes and r_s is equal to the culticular resistance (r_{s0}). The leaf water loss (W_{lloss}) is calculated based on cuticular resistance (r_{s0}; s/m) and the vapor pressure difference between leaf and air,

DOI: 10.1038/NCLIMATE2873

$$W_{lloss} = \frac{18.0}{r_b + r_{s0}} \frac{(e_s - e_a)}{RT}.$$

Table S2: Key hydraulic parameter values used for the ED model. See McDowell *et al.* (2013) for parameters of carbon dynamics and allometry.

Parameter	Description	Value for pine	Value for juniper	Sources
$\psi_{l\min}$	Minimum leaf water potential	-2.1	-4.1	Empirical
ϕ_{s0}	critical soil water potential that cause 50% loss of conductivity	-3.57	-8.45	Data
ϕ_s	shape parameter for conductivity loss	4.07	2.2	Data
A	Coefficient for xylem water potential calculation	-0.683	-1.283	(Barnard et al 2011)*
B	Coefficient for xylem water potential calculation	-0.981	-0.981	(Barnard et al 2011)+
r_{s0}	cuticular resistance (s/m)	1.0e6	1.0e6	Data
g_r	Root water loss rate (m/s/Mpa)	1.5e-10	2.5e-10	Fitted to predawn
$\psi_{sr\_\max}$	Maximum water potential gradient between soil and root (MPa)	2	3	Empirical

J. T. Ball, I. E. Woodrow, J. A. Berry, in *Progress in Photosynthesis Research,* J. Biggins, Ed. (Martinus Nijhoff Publishers, Netherlands), vol. 4, pp. 221–224. (1987)

D. M. Barnard *et al.*, Climate-related trends in sapwood biophysical properties in two conifers: avoidance of hydraulic dysfunction through coordinated adjustments in xylem efficiency, safety and capacitance. *Plant Cell Environ* **34**, 643 (2011).

H. S. Neufeld *et al.*, Genotypic variability in vulnerability of leaf xylem to cavitation in water-stressed and well-irrigated sugarcane. *Plant Physiol* **100**, 1020 (1992).

G.-Y. Niu, Z.-L. Yang, Effects of Frozen Soil on Snowmelt Runoff and Soil Water Storage at a Continental Scale. *J Hydrometeorol* **7**, 937 (2006).

J. S. Sperry, F. R. Adler, G. S. Campbell, J. P. Comstock, Limitation of plant water use by rhizosphere and xylem conductance: results from a model. *Plant Cell Environ* **21**, 347 (1998).

F. Tardieu, T. Simonneau, Variability among species of stomatal control under fluctuating soil water status and evaporative demand: modelling isohydric and anisohydric behaviours. *J Exp Bot* **49**, 419 (Mar, 1998).

C. Xu, N. G. McDowell, S. Sevanto, R. A. Fisher, Our limited ability to predict vegetation dynamics under water stress. *New Phytol* **200**, 298 (2013).

DOI: 10.1038/NCLIMATE2873

SI Figure S3. Examples of simulations used to calculate mortality probability.

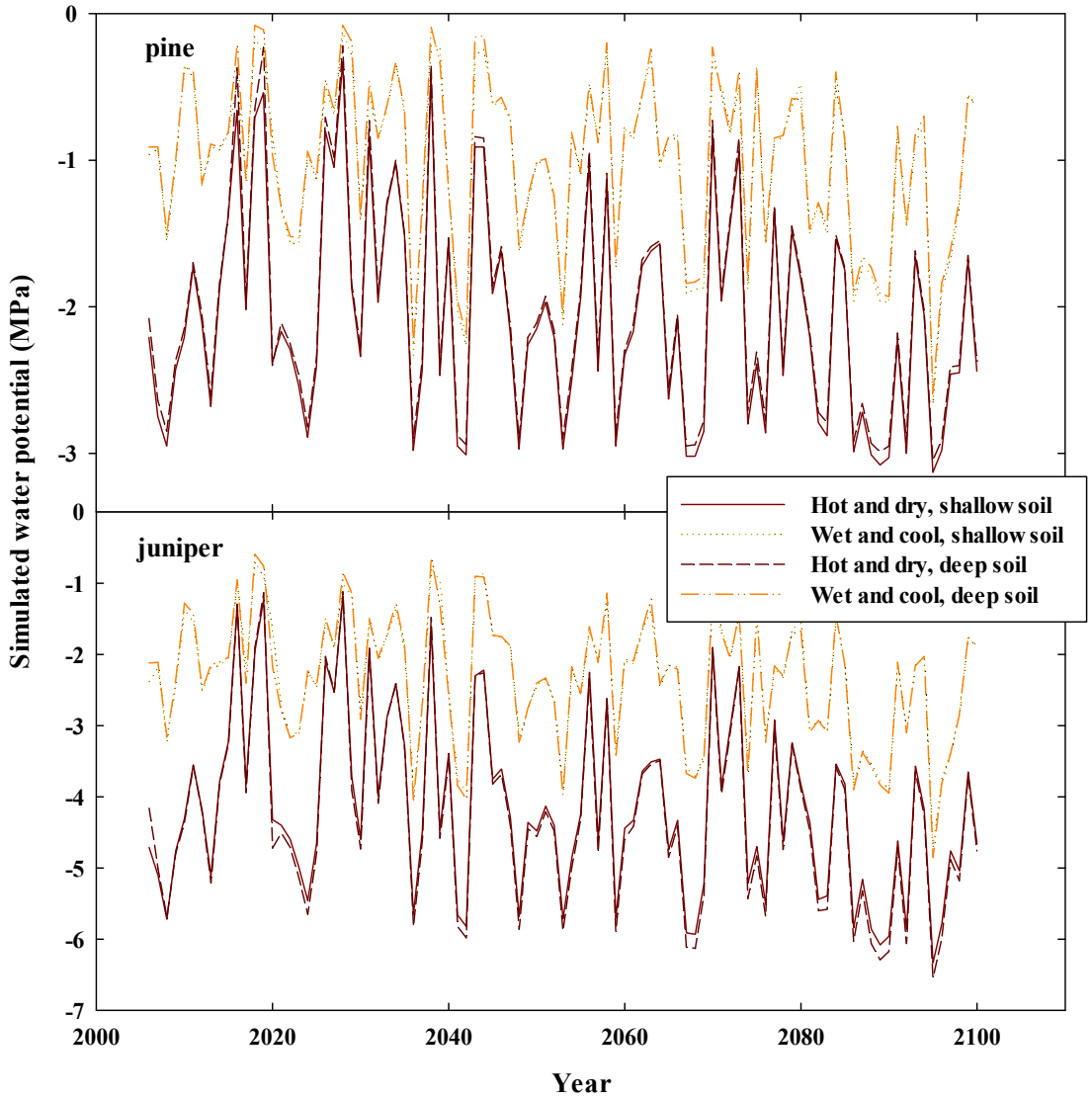

SI Figure S3. An example of the range of simulations of pre-dawn water potential (averaged for April-August) employed to calculate mortality probabilities shown in Figure 3C. In this case, MuSICA was driven with climate data from a wet and cool grid cell and a hot and dry grid cell from Figure (3D), with an assumed soil depth of either 50cm (shallow) or 150cm (deep). Climate is more important than soil depth on simulated Ψ. TREES was driven similarly. ED(X) used climate forecasts for each grid cell shown in Figure (3D) with an assumed soil depth of 50cm.

SI Figure S4. Future water potential simulations (April-August average) by each model.

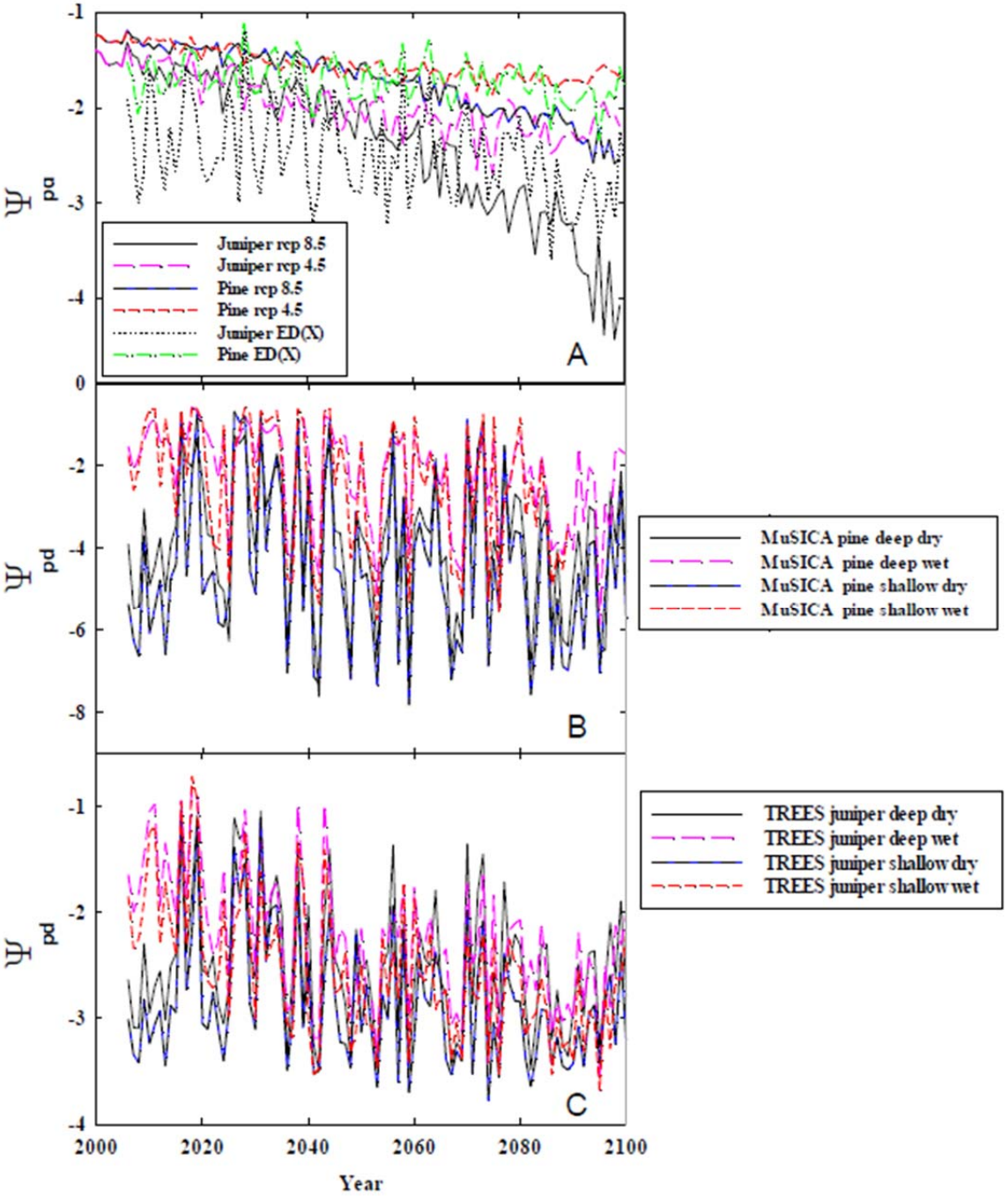

SI Figure S4 A) Simulations by the tree-ring based model for both species and for RCP 4.5 and 8.5, as well as by ED(X), **B)** simulations by MuSICA, **C)** simulations by TREES.

DOI: 10.1038/NCLIMATE2873

SI Figure S5. Survival likelihood is sensitive to origination year (2006 vs 2014).

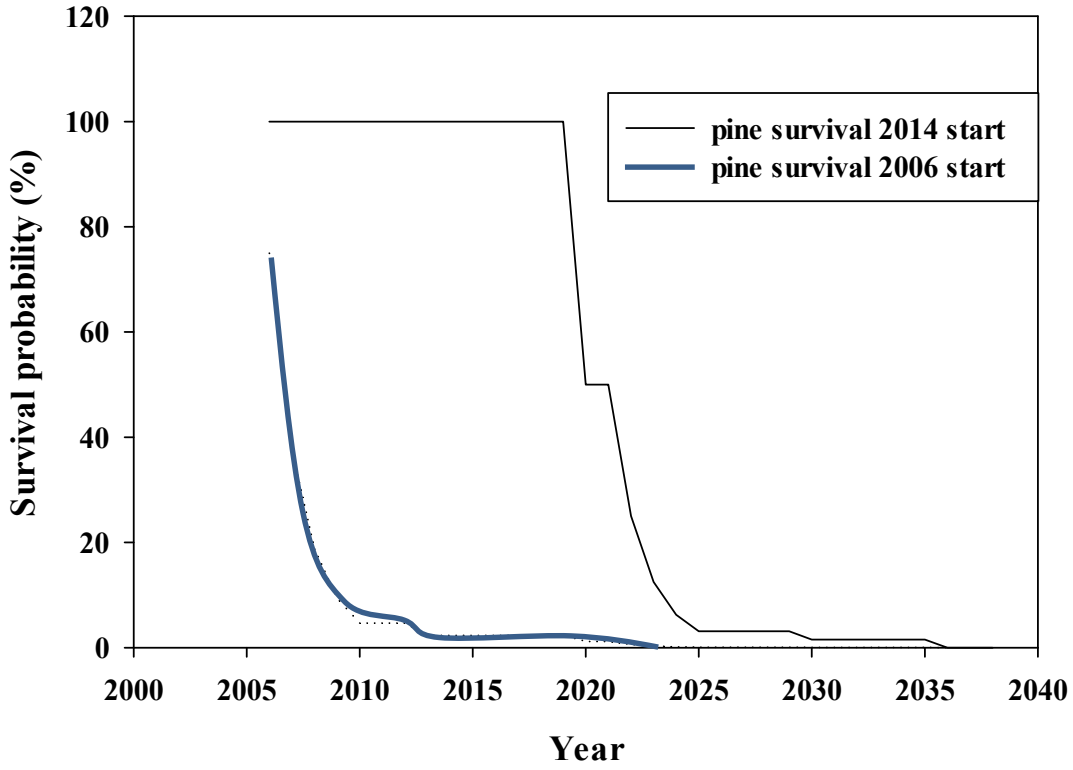

SI Figure S5. Survival probability was calculated either starting in 2006 or 2014, during the interim CMIP5 predicted multiple years of drought. Simulations are shown using the empirical model; however, all models showed the same sensitivity to the origination year of the calculations of mortality. This indicates the results presented in Figure 3C are very conservative because all model calculations of mortality probability used 2014 as a start date rather than 2006.

SI 9: In all cases future predictions of mortality relied on CMIP5 predictions of future climate. The empirical calculation used all 16 model predictions of future climate, predicted mortality probability, and then averaged them. TREES and MuSICA used a particularly hot and dry, and a particularly wet and cool, grid cell, respectively, from the CMIP5 predictions for the piñon-pine-juniper woodlands. They then assumed either 50 cm or 150 cm soil depths, respectively. The odds of Ψ crossing the species-specific thresholds were then summed across the permutations for each time step (year) and combined multiplicatively over time. ED(X) did a similar exercise but for 71 different grid cells in the piñon-pine-juniper woodland region. The empirical calculation used the CMIP5 predictions for the entire piñon-pine-juniper woodland region and equations (SI 2,3).

DOI: 10.1038/NCLIMATE2873

SI Figure S6. Comparison of mortality probability predicted by the empirical method using RCP8.5 (business as usual) vs. RCP4.5 (moderate emissions controls).

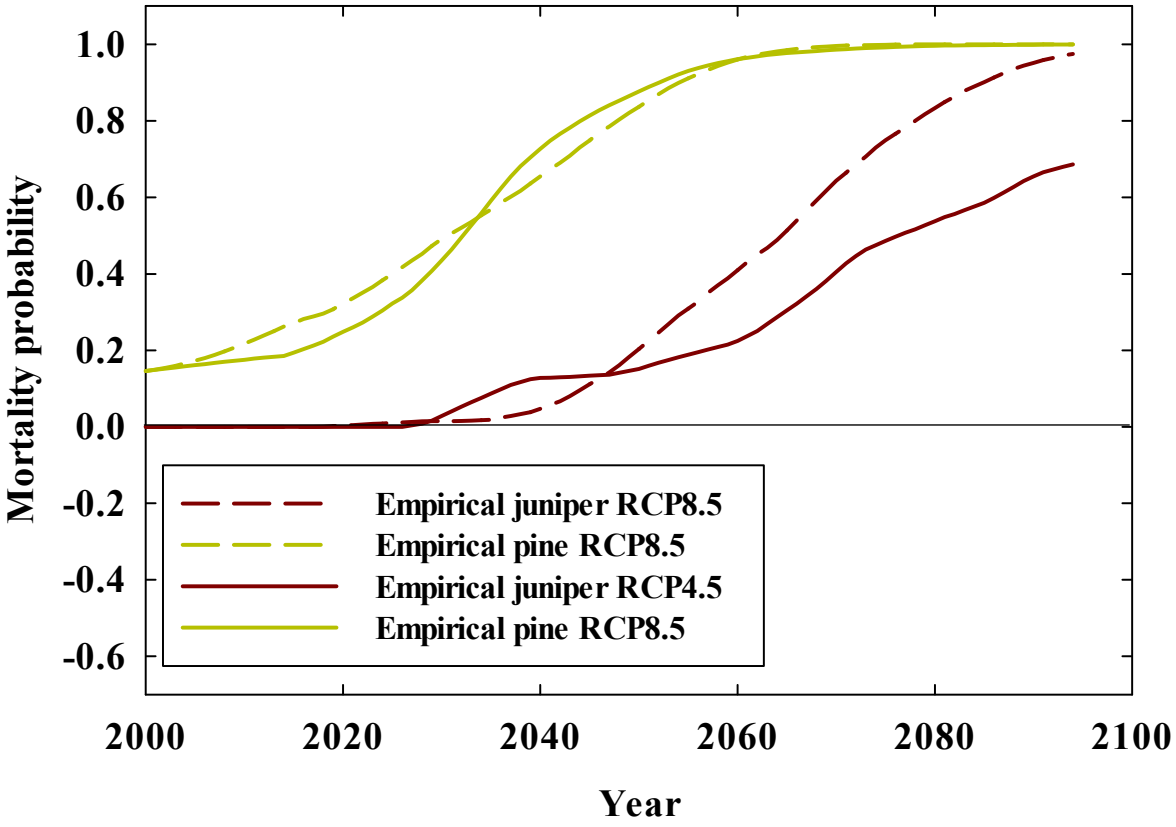

SI Figure 7. ED(X) simulations shown in Figure 3D are replicated here with the same color coding for number of mortality events between 2066-2095, except plotted here is the mean temperature and precipitation of the grid cell during that period relative to the regional means. The regression for grid cells that experienced 0-1 mortality events is: -0.007(Pr-Prregional) - 1.22 ($p<0.001$, $R^2 = 0.43$); the regression for sites that experienced greater than one mortality event is: -0.008(Pr-Prregional) + 1.70 ($p<0.001$, $R^2 = 0.20$). The dashed lines indicate the mean T-Tregional (1.95 ºC) and mean Pr-Prregional (-31.7mm) for the sites that experienced greater than one mortality event.

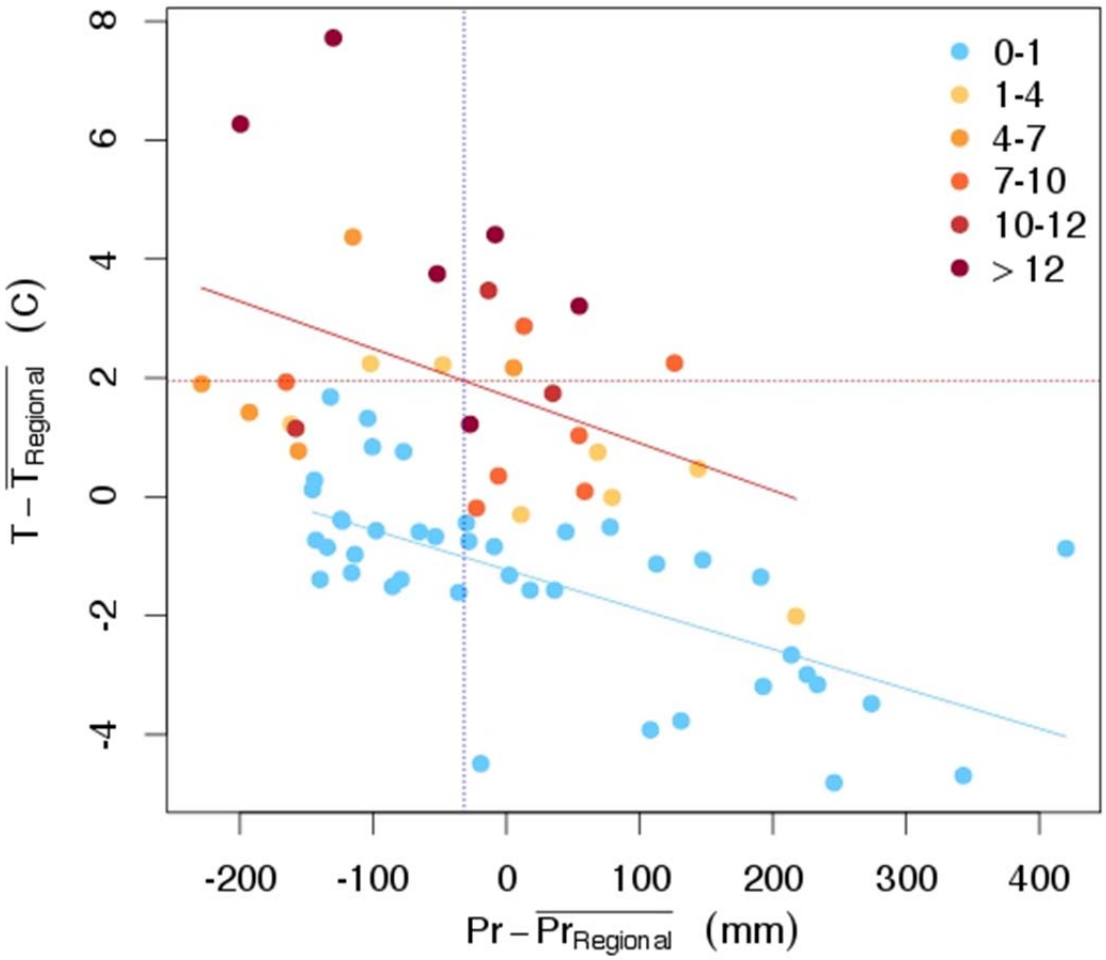

DOI: 10.1038/NCLIMATE2873

SI 10: Figure 4a-c. CMIP5 DGVM results: The changes in NET cover were calculated from three CMIP5 models that include dynamic vegetation distributions: HadGEM2-ES [TRIFFID DGVM (Cox, 2001), MIROC-ESM [SEIB-DGVM (Sato et al, 2007)], and MPI-ESM (Reick et al., 2013) models. Models are from the RCP8.5 scenario and include the percentage change in the PFT corresponding most closely to NET for each model: Needleleaf Trees (HadGEM2), Boreal Evergreen (MIROC), and Extra-tropical Evergreen Trees (MPI-ESM). Each of these models treats vegetation distributional dynamics differently: HadGEM2 uses a Lotka-Volterra approach to parameterize competition by PFTs for space and light (Cox, 2001); MIROC-ESM uses an individual-based model that considers spatially-explicit competition by PFTs for resources as well as bioclimatic limits on PFT growth (Sato et al, 2007); MPI-ESM simulates competition based on NPP (Reick et al., 2013).

There are two ways to calculate the loss and gain of NET in Figures 4A-C: (1) the total area that is gaining (blue color) and losing (red color) NET, or (2) the total area that lost and gained NET, i.e. the integral of the percentage lost and gained.

For method (1):
HadGEM2_ES lost 17.8 million km^2 and gained 20.3 million km^2;
MIROC_ESM lost 11.9 million km^2 and gained 19.4 million km^2;
MPI_ESM_MR lost 14.0 million km^2 and gained 31.8 million km^2.

For method (2),
HadGEM2_ES lost 1.88 million km^2 and gained 1.52 million km^2;
MIROC_ESM lost 2.09 million km^2 and gained 3.47 million km^2;
MPI_ESM_MR lost 0.70 million km^2 and gained 4.25 million km^2.

Figure 4d. Our simulations used the atmosphere (CAM, the Community Atmosphere Model) and land surface components (CLM, the Community Land Surface Model) of the Community Earth System Model (CESM). For the atmosphere, we employed the finite volume (FV) dynamical core and CAM version 4 physics with 26 vertical levels (Neale et al. 2010). The spatial resolution of the model is 1.9° latitude by 2.5° longitude. Exchanges of heat, moisture, and momentum fluxes between the land and the atmosphere are simulated by the land surface model, CLM, version 4.0. In CLM4.0, vegetation coverage is described in each grid cell by fractional areas of plant functional types (PFTs). There are 17 PFTs including bare ground, 11 tree PFTs, three grass PFTs, and two crop PFTs. CLM4.0 includes a carbon-nitrogen (CN) biogeochemical model that predicts vegetation, litter, soil carbon and nitrogen states, and vegetation phenology (Thornton *et al.* 2007). The dynamic vegetation is based on the Lund-Potsdam-Jena (LPJ) model (Sitch *et al.* 2003), wherein vegetation change is represented by a change in the fractional PFT coverage of a grid cell at the end of each year (Sitch *et al.* 2003). The LPJ dynamic component in CLM4.0 is among the most mechanistic of the existing DGVMs (McDowell *et al.* 2011). Plant functional types can change according to twenty-year climate envelopes based on temperature and precipitation limits as well as due to mortality mechanisms. Mortality can occur due to heat stress (based on an accumulation of growing degree days), fire, and growth efficiency. In our simulations, the interaction between the land and atmosphere components is two-way, unlike previous studies performed to evaluate the basic performance of CLM in CESM (*e.g.*, Gotangco Castillo *et al.* 2012).

The sea surface temperature data used as boundary conditions include results from simulations of 21st century climate under a medium-high emissions range (Special Report on Emissions Scenarios A1B, (Nakicenovic *et al.* 2000)). Output from the following eight models in the Coupled Model Intercomparison Project version 3 (CMIP3) (Meehl *et al.* 2007) were used: the National Center for Atmospheric Research Community Climate Model, version 3 (NCAR-CCSM3); Météo-France / Centre National de Recherches Météorologiques Coupled Global Climate Model, version3 (CNRM-CM3); Max Planck Institute for Meteorology ECHAM5 (MPI-ECHAM5); Geophysical Fluid Dynamics Laboratory Climate Model version 2.1 (GFDL-CM2-1); Goddard Institute for Space Studies Model R, coupled with Russell ocean component (GISS-ER); Hadley Centre Coupled Model, version 3 (UKMO-HadCM3); Hadley Centre Met Office Hadley Centre Global Environmental Model, version 1 (UKMO-HadGEM1); and Meteorological Research Institute Coupled Atmosphere- Ocean General Circulation Model, version 2.3.2 a (MRI-CGCM2.3A).The CESM simulations employed here proved accurate for simulating the current vegetation coverage in North America (Jiang et al. 2013).

Cox, P. M. Description of the TRIFFID dynamic global vegetation model, *Hadley Centre Technical note*, *24* (2001).

Gotangco Castillo, C. K., S. Levis, and P. Thornton, Evaluation of the new CNDV option of the Community Land Model: Effects of dynamic vegetation and interactive nitrogen on CLM4 means and variability. *J. Climate*, **25**, 3702–3714. (2012)

McDowell, N.G., D. Beerling, D. Breshears, R. Fisher, K. Raffa, M. Stitt. Interdependence of mechanisms underlying climate-driven vegetation mortality. *Trends in Ecology and Evolution*, **26,** 523-532. (2011)

Meehl, G. A., C. Covey, K. E. Taylor, T. Delworth, R. J. Stouffer, M. Latif, B. McAvaney, J. F. B. Mitchell, The WCRP CMIP3 multimodel dataset: A new era in climate change research. *Bull. Amer. Meteor. Soc.*, **88**, 1383–1394. (2007)

Nakićenović, N., *et al*, Special Report on Emissions Scenarios. Cambridge University Press, 570 pp. (2000)

Neale, R. B., et al, Description of the NCAR Community Atmosphere Model (CAM 4.0). NCAR Tech. Note NCAR/TN-485+STR, 212 pp. [Available online at http://www.cesm.ucar.edu/models/ccsm4.0/cam/docs/description/cam4_desc.pdf.] (2010)

Reick, C. H., T. Raddatz, V. Brovkin, and V. Gayler, Representation of natural and anthropogenic land cover change in MPI-ESM, *Journal of Advances in Modeling Earth Systems*, **5**(3), 459-482. (2013)

Sato, H., A. Itoh, and T. Kohyama, SEIB–DGVM: A new Dynamic Global Vegetation Model using a spatially explicit individual-based approach, *Ecological Modelling*, **200**(3–4), 279-307. (2007)

DOI: 10.1038/NCLIMATE2873

Sitch, S., *et al.*, Evaluation of ecosystem dynamics, plant geography and terrestrial carbon cycling in the LPJ dynamic global vegetation model. *Global Change Biol.*, **9**, 161–185. (2003)

Thornton, P. E., J. F. Lamarque, N. A. Rosenbloom, and N. M. Mahowald, Influence of carbon-nitrogen cycle coupling on land model response to CO_2 fertilization and climate variability. *Global Biogeochem. Cycles, 21*, GB4018, doi:10.1029/2006GB002868. (2007)